Fission-Antineutrino Interaction with Protons*

F. A. NEZRICK†‡ AND F. REINES
Department of Physics, Case Institute of Technology, Cleveland, Ohio
(Received 27 September 1965)

The positron kinetic-energy spectrum from the antineutrino absorption reaction $p(\bar{\nu}_e,\beta^+)n$ was measured by using a 3.2-liter gadolinium-loaded decalin-based liquid-scintillator target placed between two cylindrical NaI crystals 29 cm in diameter and 7.6 cm thick. The crystals were set to see 0.51-MeV β^+ annihilation radiation. A prompt triple coincidence of all three detectors followed by the delayed capture of the neutron is the signature for the reaction. The experiment was performed at one of the powerful fission reactors of the Atomic Energy Commission's Savannah River Plant. The data were obtained during 2484 h of operation at the rate of 0.187 events per hour, with a signal-to-background ratio of approximtely 3/1. The antineutrino spectrum from U^{235} fission gave evidence for a higher energy tail than previously known, implying the presence of half-lives in the several-millisecond range. The cross section per fission antineutrino for the inverse beta decay of the proton was measured to be $(0.94\pm0.13)\times10^{-43}$ cm^2, a value consistent with the two-component theory of the neutrino. The measured antineutrino spectrum indicates an expected cross section for the reaction $d(\bar{\nu}_e,\beta^+)2n$ of $(4.2\pm1.4)\times10^{-45}$ cm^2/(fission $\bar{\nu}_e$) and a cross section of $(8.4\pm2.8)\times10^{-46}$ cm^2/(fission $\bar{\nu}_e$) for the production of >1.5-MeV recoil electrons by the elastic scattering reaction $\bar{\nu}_e+e^-$.

INTRODUCTION

A PREVIOUS investigation[1] of the reaction

$$\bar{\nu}_e+p\rightarrow\beta^++n \qquad (1)$$

using reactor antineutrinos showed that the reaction cross section is consistent with the two-component neutrino theory,[2] but with marginal accuracy. The positron kinetic energy spectrum, and hence the antineutrino spectrum from fission fragments were only crudely determined in this earlier work which was designed primarily to obtain a somewhat improved value for the cross section. A liquid scintillation detector[1] gave a delayed coincidence pair, in which the first pulse was proportional to the sum of the positron kinetic energy and the energy of the positron annihilation gamma rays which were superimposed because the positron slowed down and annihilated within the resolution time of the system and the entire phenomenon occurred in one detector. The accuracy of the spectrum obtained from this arrangement was limited by the uncertainty in the leakage of the annihilation gamma rays from the detector and its poor energy resolution (±25% for 1 MeV deposited). The cross section was determined to ±25%. The signal-to-background ratios were: 2/1 for reactor-associated accidental background and $\frac{1}{5}$ for the total reactor-independent background.

The present experiment has much improved energy resolution, (±12% at 1 MeV), because it measures the annihilation gamma rays in NaI(Tl) detectors and the positron kinetic energy in a detector with increased photon collection. Figure 1 is a schematic of the detector. Further, the signal-to-background ratio is much more favorable:

$$\text{Reactor-independent: } \frac{\text{Signal}}{\text{Correlated background}}=5.5$$

$$\frac{\text{Signal}}{\text{Accidental background}}=4.8$$

$$\text{Reactor-associated: } \frac{\text{Signal}}{\text{Accidental background}}=4.3.$$

In addition it was possible to determine the detection efficiency with improved accuracy (±12%).

The proton target is a squat cylinder of liquid scintillator loaded with gadolinium to capture the product neutron and provide several energetic gamma rays. A NaI crystal is located on each side of the target detector. Figure 1 illustrates reaction (1) as detected by this system. The positron slows down ($\sim10^{-10}$ sec) within the resolution time of the electronics (~1.5 μsec) and annihilates so that a prompt triple coincidence is observed. The energy pulses from the two NaI crystals are individually 0.51 MeV and the energy pulse from the liquid scintillator is due to the kinetic energy of the positron. The neutron thermalizes in the hydrogenous scintillator and is captured by the gadolinium which produces on the average four gamma rays, each with a mean energy of ~2 MeV.[3] These gamma rays can interact in one, two, or three of the detectors. Reaction (1), then, has for a signature a prompt triple coincidence produced by the positron followed by a delayed pulse (or coincident pulses) produced by the neutron capture gamma rays. In this detection scheme, the background is greatly reduced by requiring that the NaI pulses of the prompt triple coincidence fall within a narrow energy window centered at the annihilation gamma-ray energy.

* Supported in part by the U. S. Atomic Energy Commission.
† This paper is based on a thesis submitted in partial fulfillment of the requirements for the degree of Doctor of Philosophy at Case Institute of Technology.
‡ Present address: CERN, Geneva, Switzerland.
[1] F. Reines and C. L. Cowan, Jr., Phys. Rev. **113**, 273 (1959).
[2] T. D. Lee and C. N. Yang, Phys. Rev. **105**, 1671 (1957).
[3] *The Reactor Handbook* (Interscience Publishers, New York, 1962), Vol. 3, p. 46.

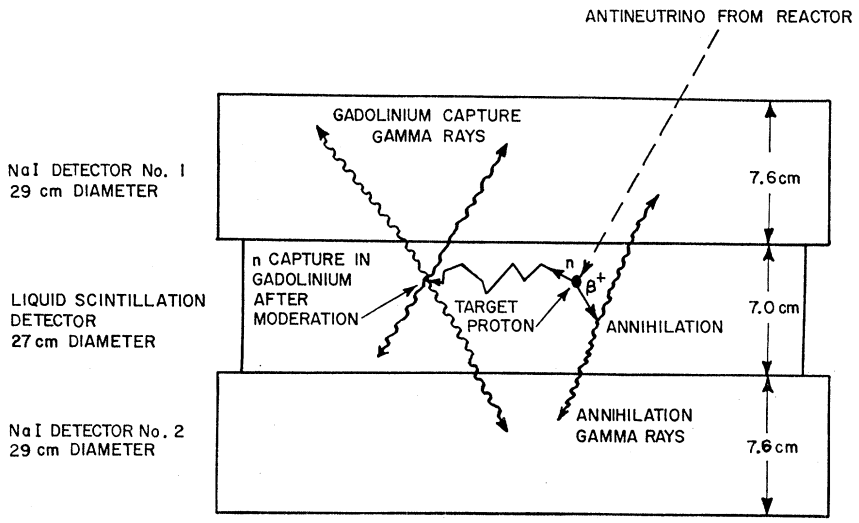

FIG. 1. Schematic diagram of the antineutrino detection scheme.

The NaI crystal[4] diameter of 29 cm was fixed by the state of the art of crystal growing. Since the NaI crystals are used to detect 0.51-MeV gamma rays (absorption mean free path of 6.8 cm in NaI), a thickness of 7.6 cm was considered sufficient.

The liquid-scintillator thickness was chosen with a view to maximizing the signal rate and the probability of absorbing the positron, subject to the requirement that the annihilation gamma rays be transmitted without interacting. Appendix I shows that the optimum thickness is from 6 to 10 cm.

Decalin[5] ($C_{10}H_{18}$) was chosen as the scintillator solvent because of its high proton density (6.9×10^{22}/cm^3). The decalin was decolored and loaded with 2.0 g/l *p*-terphenyl as the primary scintillator solute, 4.0 g/l alpha-naphthyl-phenyloxazole as the wavelength shifter and 24 g/l of gadolinium 2-ethylhexate[6] to capture the neutron. The liquid scintillator was contained in a right circular Lucite cylinder which was viewed on its vertical wall by 13 CBS 7817 (2-in.) photomultiplier tubes.[7]

In order to reduce the gamma-ray background from the reactor, it was necessary to enclose the detector in a lead house which ranged in thickness from 30 to 40 cm and weighed 30 tons. In addition it was necessary to place a paraffin-borax neutron shield around the detector elements inside the lead house. This composite shield reduced the "reactor-up" background seen by one of the NaI crystals by a factor ranging from 4400 at 1 MeV to 44 000 at 6.5 MeV so that the reactor-up spectrum in the shield was approximately 10% higher than the "reactor-down" spectrum for gamma ray energies below 3.0 MeV.

The data were in the form of photographed oscilloscope traces. Since there were three detectors which had doubly differentiated amplifier outputs and only one oscilloscope beam, the pulses were coded to enable identification of the associated detector. The liquid-scintillator pulses were retained as doubly differentiated while the pulses from the NaI amplifiers were diode biased so that only the positive and negative halves were retained for NaI 1 and NaI 2, respectively. Since both the prompt and delayed signals can be threefold coincidences, the amplifier outputs were "separated in time" by driving their pulses through different length delay lines prior to display on the oscilloscope. A typical display is illustrated in Fig. 2. In the figure, h_1, h_3, and h_5 (where $h_3=h_5=0.51$ MeV) form the threefold prompt coincidence signal, while h_2, h_4, and h_6 (where only one need be nonzero) form the coincidence delayed signal produced by the neutron capturing at a time t_c from its birth. The oscilloscope display was photographed every time a proper prompt signal occurred, approximately at the rate of 28 per hour. The film was later scanned for delayed pulses appropriate to neutron capture. Such delayed coincidences occurred at the rate of $\sim$0.25 per hour.

The data collected during 2484 h of reactor-up time and 356.8 h of reactor-down time satisfied the following criteria:

(a) The positron kinetic energy, h_1, must be >0.50 MeV. This threshold was necessary because of the rapidly rising background below 0.50 MeV.

(b) The oscilloscope was triggered only when the prompt signal was characteristic of a positron annihilation; i.e., the NaI crystals must observe gamma rays in the vicinity of 0.51 MeV. Therefore, $h_3=h_5=0.51$

[4] The NaI(Tl) crystals are from the "Matched Window Line" of the Harshaw Chemical Company, Cleveland, Ohio, and contained low background tube bases.

[5] First demonstrated to be a scintillator solvent by C. L. Cowan.

[6] The gadolinium 2-ethylhexate was supplied by the Pilot Chemicals Inc., Watertown, Mass.

[7] There is a variation in minimum photocathode areas of 2-in.-diam. photomultiplier tubes depending on the manufacturer. The minimum photocathode areas for Dumont 6292 and CBS 7817 are, respectively, 1.76 in.^{2} and 2.39 in.^{2}. 13 CBS tubes are therefore equivalent in photocathode area to 17.7 Dumont 6292 tubes.

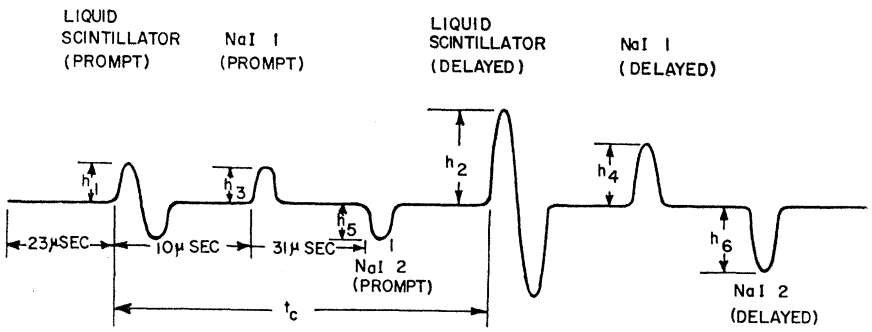

FIG. 2. Illustration of a typical oscilloscope trace showing a prompt and delayed signal.

MeV±the crystal resolution. However, most of the oscilloscope triggers were not due to positrons since the system did not discriminate sufficiently against correlated energy losses which met the trigger requirements.

(c) The sum of the energy deposits in the delayed pulse must be greater than 0.75 MeV.

(d) The neutron must capture within the time gate of $2.8 \leq t_c < 100$ μsec.

(e) Oscilloscope traces were rejected if more than one neutron-like pulse was observed or if any pulse occurred before the prompt signal.

Requirements (c) and (d) served to distinguish neutrino-produced triggers. The delayed coincidence data were divided into two groups of 50 μsec each. Since the liquid scintillator was measured to have a mean life of 8.0 μsec for neutron capture, most of the neutrons were captured within the first group ($0 \leq t_c \leq 50$ μsec). The second group gave the accidental delayed-coincidence background. Subtracting the rate in the second group from the rate in the first we obtained the correlated reactor-up (100% power) signal. A similar determination with the reactor down gave the correlated reactor-down (0% power) signal. The correlated reactor-associated signal rate is the difference between the correlated reactor-up and reactor-down rates.

To complete the experiment, tests were performed to verify that

(a) The reactor-associated signal is correlated and hence is not due to the increase in the accidental background.

(b) The second pulse results from neutron capture.

(c) The first pulse is characteristic of a positron.

On the basis of these tests and an argument ruling out neutrons as a background for reaction (1) it was concluded that the observed signal is due to reactor antineutrinos through the inverse beta decay depicted in Eq. (1).

In a determination of the positron, and hence $\bar{\nu}_e$, spectrum, it is necessary to know the variation of detection efficiency with $\bar{\nu}_e$ energy. The positron detection efficiency was both calculated and measured. The neutron detection efficiency was calculated by Monte Carlo techniques. The over-all detection efficiency is the product of these two.

The reactor-associated positron spectrum was obtained by folding the detector resolution and efficiency with a two-parameter function which has the general shape of the expected spectrum. The parameters were determined by a least squares fitting to the data of the expected spectrum as distorted by the detector response. The unnormalized fission antineutrino spectrum was obtained from the unfolded positron spectrum by taking the energy dependence of the cross section as given by phase-space arguments[8] and normalization was accomplished by a comparison with the measured spectrum of betas from fission.

The significance of this $\bar{\nu}_e$ spectrum for other reactor antineutrino experiments and the fission process itself is discussed and, finally, the average cross section per fission antineutrino is seen to compare well with the value expected from the two component theory and the half-life of the neutron.

EXPERIMENTAL ARRANGEMENT

The feasibility of the present approach was tested by measurements made with a mockup at one of the Savannah River Plant reactors. The mockup was composed of two NaI crystals 12.5 cm diam by 5.1 cm thick and a plastic scintillator 7.6 cm diam by 5.1 cm thick observed by two phototubes placed radially and at right angles to each other. Encouraged by these results and guided by a background survey we constructed a full-size detection system and a 30-ton lead house.

The detector elements were mounted within the lead house and were accessible through an electrically operated 4-ton door.

The preamplifiers, high-voltage distribution box and a two-way communication system were mounted on top of the house. The experimental area and electronics area were connected by 95 m of doubly shielded signal, high voltage and intercommunication cables carried in a shielded cable tray. The electronics are of conventional (~0.2 μsec rise time) design.

Lead House

To determine the thickness of the lead shield needed to reduce the background to acceptable levels, a survey

[8] L. Heller, Los Alamos Laboratory Report No. 3013, 1964 (unpublished).

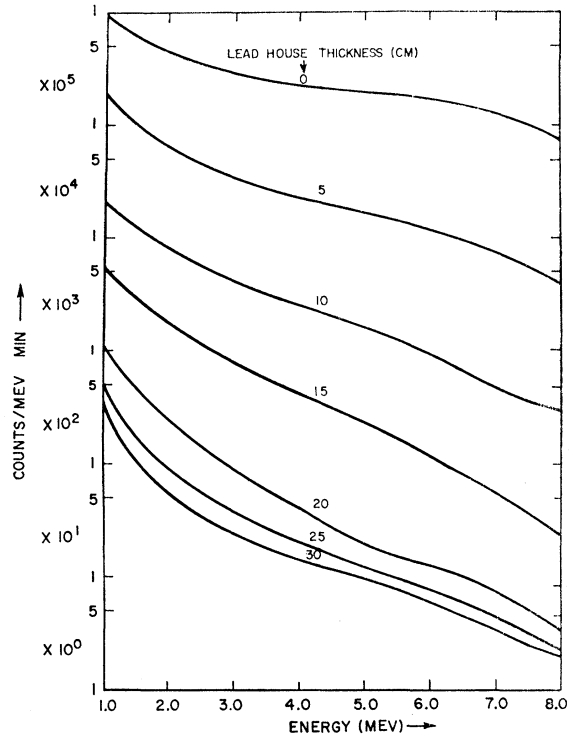

FIG. 3. Background reduction versus lead house thickness.

was made with a 12.5-cm-diam, 10-cm-thick NaI crystal. The gamma-ray background spectrum was measured, with the reactor at full power, from 0.20 to 8.0 MeV as a function of the thickness of a lead shield placed around the crystal. The effects of varying the shield thickness from 0 to 30 cm on the high-energy spectrum from 1.0 to 8.0 MeV is shown on Fig. 3. Figure 4 shows the low-energy spectrum from 0.20 to 0.80 MeV for a shield thickness of 30 cm compared with the spectrum measured in the low-background Case Institute laboratory located in the Morton Company Painesville, Ohio salt mine. The salt mine is the least radioactive experimental area encountered by the Case neutrino group and therefore suggests a limit for the obtainable background.

Figure 3 indicates that there were neutrons in the area which gave rise to background via capture gamma rays since the background did not decrease sufficiently rapidly for increasing shield thicknesses greater than 20 cm. It was therefore decided to build a 30- to 40-cm-thick lead house plus a neutron shield to reduce the background.

An aluminum liner was placed in the detector cavity. This liner had three sets of slides on which the three detectors were placed. The neutron shield was stacked within the aluminum liner in two concentric 7.6-cm-thick shells. The outer shell, the neutron moderator, was paraffin; and the inner shell, the neutron absorber, was borax. Ideally, the neutrons should have been captured exterior to the gamma shield but this was not possible because of space limitations.

Detector Elements

NaI Crystals

The crystal detectors are NaI(Tl) crystals 29 cm in diameter by 7.6 cm thick of the Harshaw matched window line housed in 0.048 cm of stainless steel. Each crystal assembly is viewed by 7 Mumetal shielded RCA 3-in. diam photomultiplier tubes with low background tube base assemblies and was mounted on a 58-cm-square aluminum tray.

Since every photomultiplier tube has an individual high voltage fine adjustment to balance its gain, it was possible to use a common high voltage. The outputs of all seven tubes on each detector were fed to a common cable. The signal and high-voltage yokes were designed to produce a minimum amount of connector noise and also to occupy a minimum amount of space within the shield. The signal and high-voltage yokes on each

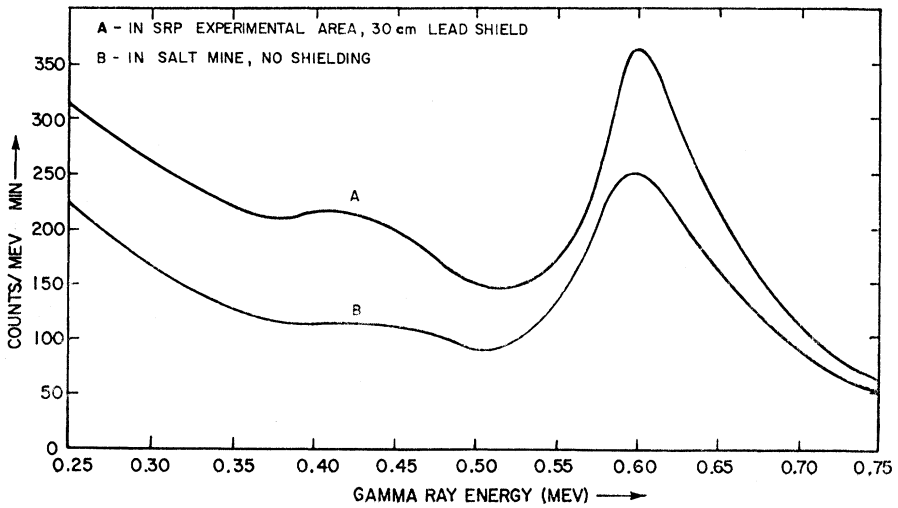

FIG. 4. Comparison of low-energy background spectra.

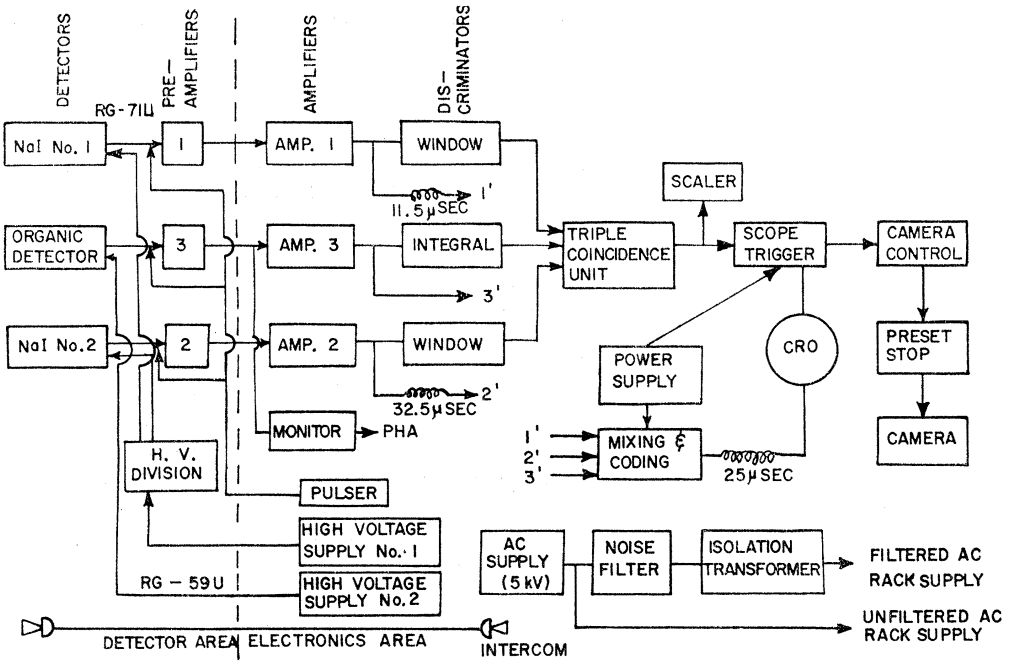

FIG. 5. Schematic diagram of detector and associated electronics.

crystal use one BNC signal T and one BNC high-voltage T connector on each tube. A high-voltage unshielded cable is soldered so as to connect the center conductors of adjacent T connectors. Over this cable were placed an insulator and two layers of braided shielding. The two layers of braid are soldered to the outside of the T connectors and the yoke was made moisture proof by shrinking a piece of plastic tubing over the braid.

The Liquid Scintillation Target Detector

This detector was 3.7 liter of decalin-based liquid scintillator contained in a right circular Lucite cylinder and viewed on its vertical wall by photomultiplier tubes.

The side wall of the cylinder and end covers are, respectively, 0.95 cm and 0.16 cm thick. There are 13 flats of width 5.4 cm cut equally spaced around the periphery of the detector to accommodate the photomultiplier tubes. It was found at a later date that the scintillator attacked the lucite and became less transparent. To prevent this deterioration of the scintillator, the entire inside surface of the lucite detector was covered with pieces of $\frac{1}{2}$ mil Mylar film. The detector was filled through a 1.2 cm diam hole in the center of the top cover.

The liquid scintillation detector was rigidly fixed in a housing which consisted of an aluminum cylinder 36 cm in diameter by 8.3 cm high and was mounted on a sliding aluminum tray for ready access. The thirteen mumetal shields are epoxied to the detector housing and a felt pad was cemented inside each mumetal shield so that a 2-in.-diam phototube was held firmly centered in the shield. The phototubes were optically coupled to the polished flats on the detector wall with Dow Corning QC 2-0057 coupling grease and were spring loaded to keep them firmly seated against the detector flats thus insuring a good optical coupling. The inside of the aluminum detector housing including the mumetal shields were painted white[9] to enhance photon collection. Dust covers, made of 1-mil Mylar sheets painted white and mounted on metal rings, were inserted in the top and bottom of the aluminum housing. In addition to preventing foreign matter from collecting on the detector and altering its total internal reflection properties these dust covers were also found to help smooth out the dependence of pulse height on the radial position of the scintillation.

Electronics and Data Recording

A schematic diagram of the detector and associated electronics is shown in Fig. 5. The scintillation light produced in the detectors is converted into electrical signals by the photomultiplier tubes mounted on each detector. The photomultiplier-tube outputs are matched to the 100-Ω characteristic impedance of the signal cable, RG 71U, by the preamplifier driving 95-m cables which deliver the signals to the electronics area for further amplification by doubly differentiated amplifiers. The amplifier outputs are fed into pulse-height selectors, whose triggered outputs are tested for the prompt triple coincidence which is characteristic of a signal. Upon receiving a triple coincidence, the coincidence unit triggers the oscilloscope and the camera control circuit, i.e., the camera shutter is opened, the

[9] Placite 7133 paint was supplied by Wisconsin Protective Coating Company, Green Bay, Wisconsin.

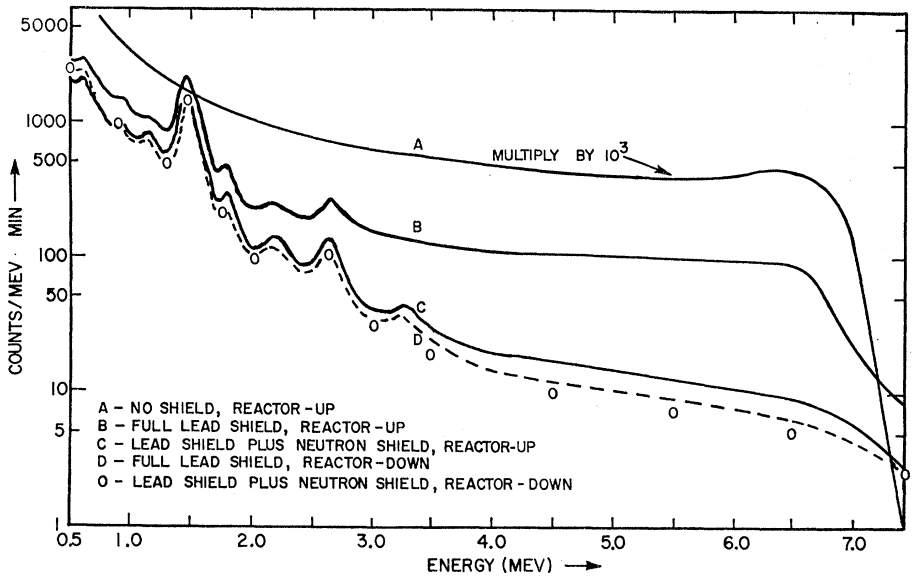

FIG. 6. Background measured inside the lead shield by the 29×7.6 cm NaI crystal.

oscilloscope sweeps 10 cm at 20 μsec/cm, the shutter closes, the film advances and the frame number and time are photographed on the top of the *next* frame.

During the process of determining whether the prompt signal meets the selection criteria, the pulses from the three amplifiers pass through delay lines, are coded, are mixed together on a single line and are stored in an additional delay line. If the selection criteria are satisfied, then the information stored in the delay line is displayed on the oscilloscope and photographed. As seen from the illustration of the oscilloscope display (Fig. 2), the coding of the pulses is achieved by diode-biasing the amplifier outputs so that NaI 1 only has a positive pulse and NaI 2 has only a negative pulse while the pulse from the liquid scintillator has both positive and negative excursions. The camera control circuit activates the preset stop circuit which automatically cuts off the camera power after a preset number of photographs have been taken. This prevents the camera from running out of film and, because of a peculiarity of its design, overheating.

Since the two NaI crystal detectors had different intrinsic gains, it was necessary to operate them at two different high voltages, a condition which was met by using one high-voltage supply and a distribution circuit. This circuit was mounted on top of the lead house along with a meter which monitored the high voltage. A glance at the monitor sufficed to tell if the high voltage was turned on or off before working inside the lead shield where exposed high voltage lines existed.

The ac power in the electronics racks was divided into an isolated filtered line and an unfiltered line. All of the electrically noisy gear were operated off the unfiltered line, e.g., camera, preset stop circuit, and rack blowers. All other electronic circuits used the isolated filtered power.

The data in the form of oscilloscope traces were photographed using 100-ft rolls of 35 mm Kodak Royal X Pan recording film.[10] Each roll of film contained 1725 pictures which represented an accumulation of about 65 h of reactor-up data. The film developed in Kodak DK 60a developer for 10 min at 68° F with constant agitation gave good but not excellent results.[11] The quality of the photographs was limited because the 3-kV cathode ray tube of the oscilloscope could not produce a well-focused intense trace at a writing speed of 20 μsec/cm. The ultra-fast film required was very grainy and had a noticeable fog intensity. The film was scanned and analyzed on a Recordak film reader.

BACKGROUNDS

The background measured within the shield is given in Fig. 6 by spectrum B and spectrum D for the reactor at full power and zero power, respectively. The full-power spectrum measured within the shield was greater than calculated from the unshielded crystal spectrum and the lead house thickness. As indicated earlier this suggested that there were neutrons in the area and that since these neutrons were relatively unaffected by the lead shield, they captured within it producing gamma rays.

The addition of a paraffin-borax neutron shield, which was capable of absorbing neutrons by nonradiative capture, reduced the spectrum within the lead house to spectrum C in Fig. 6. The existence of a residual difference between the reactor-up and the reactor-down spectra suggests that a better shield could be built. Also, since the reactor-off spectrum was decreased by the neutron shield, we conclude that cosmic-ray neutrons are a source of background.

[10] Kodak Royal X Pan recording film was used because it was the fastest (ASA of 1250) 35 mm film supplied on 100 foot rolls.

[11] It was subsequently learned that D76 developer gives better results.

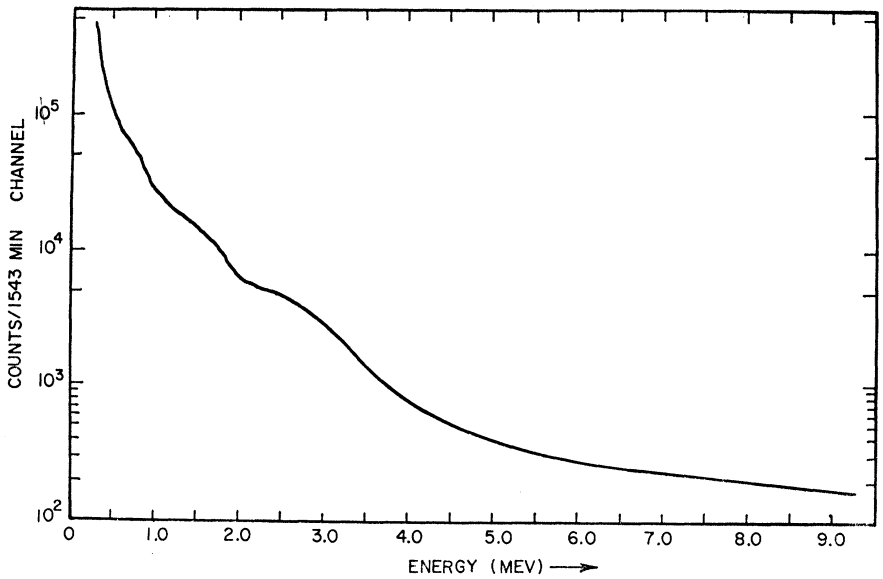

FIG. 7. Reactor-up spectrum observed by target detector.

The background below 3.5 MeV within the shield is produced primarily by the natural radioactivity of the detectors and shield. The peaks in the background spectrum result from the K^{40} in the photomultiplier tube glass and socket, and the thorium (Th*C*, Th*C''*) and uranium series (Ra*C*).[12]

The background observed by the liquid-scintillation detector within the lead and paraffin-borax shield with the reactor at full power is given in Fig. 7. The background rates within the shield for the component detectors is given in Table I.

TABLE I. Component detector rates.

Detector and energy requirements	0% power	100% power
NaI 1 window	210/min	250/min
NaI 2 window	200/min	250/min
Organic detector >0.40 MeV	1100/min	1300/min
NaI 1—NaI 2 coincidence	···	1.0/min
Triple coincidence	(5.6±0.3)/hour	(28.2±0.7)/hour
NaI 1 or NaI 2 >0.75 MeV	850/min	1000/min
Organic detector >0.75 MeV	650/min	760/min

DETECTOR PROPERTIES

NaI Crystals

The prime function of the NaI crystals was to detect annihilation gamma rays with good energy resolution thus allowing a discriminator with a very narrow window to be used to discriminate against backgrounds not due to positrons. To determine the minimum useful width of the window, the variations in photopeak position and resolution were measured for a Cu^{64} positron source which was placed at various radial positions. Table II gives the results of these measurements for both crystals. Since the peak position and the resolution (full width at half maximum) were measured with a pulse-height analyzer, the uncertainty in these values is one analyzer channel. It is seen that no variations were observed within statistical fluctuations. The resolutions for 0.51-MeV gamma rays absorbed by NaI 1 and NaI 2 are, respectively, 9.3±0.3% and 10.4±0.3%.

The energy calibration of the crystals using the photopeaks of Cu^{64} (0.51 MeV), Cs^{137} (0.662 MeV), and Y^{88} (0.90 MeV), 1.85 MeV, and their sum of 2.76 MeV) showed that the crystal responses were linear.

TABLE II. Photopeak properties for 0.51-MeV gamma rays in NaI detectors.

Radial position (cm)	NaI 1 Peak channel	NaI 1 FWHM (channels)	NaI 2 Peak channel	NaI 2 FWHM (channels)
1.3	178.5±1	16.5±0.5	155.0±1	15.5±0.5
5.1	178.5±1	16.5±0.5	154.5±1	16.0±0.5
8.3	177.0±1	17.0±0.5	154.0±1	16.0±0.5
10.0	176.5±1	16.5±0.5	154.0±1	16.0±0.5
12.0	176.5±1	16.5±0.5	154.0±1	16.5±0.5

The Organic Detector

The resolution function and energy calibration of the liquid scintillation detector were measured so the true positron spectrum could be deduced from the observed spectrum. The energy dependence of the resolution function was obtained from pulse-height analysis of the detector response to an electron source. The source used

[12] R. D. Evans, *The Atomic Nucleus* (McGraw-Hill Book Company Inc., New York, 1955), p. 517.

was Bi^{207} which undergoes K capture[13] to excited states of Pb^{207}. The 0.569-MeV and 1.064-MeV gamma rays from the excited levels of Pb^{207} produce K conversion electrons of 0.477 MeV and 0.972 MeV in cascade with 1.064-MeV and 0.569-MeV gamma rays, respectively. The 0.477-MeV or the 0.972-MeV conversion line spectra were selectively obtained by immersing the Bi^{207} source into the liquid scintillator and by requiring a coincidence between the liquid scintillator and one of the NaI crystals, where the crystal was set to see energy deposits of 1.064 MeV or 0.569 MeV, respectively. The discriminator on the crystal output supplied the coincidence gate pulse for the pulse-height analyzer which analyzed the liquid-scintillator output pulses.

Since the K conversion coefficients are 0.113 and 0.018 for the 1.064-MeV and 0.569-MeV gamma rays, respectively, it was possible for the unconverted gamma rays to interact in the organic detector and produce false electron signals whose coincidence with the cascade gamma ray seen by the NaI would distort the line spectrum accumulated on the pulse-height analyzer. To compensate for this effect, an equal live-time background subtraction was made with an 80-mil-thick high-Z shield covering the source. Since this shield was thicker than the 3.54-MeV electron range, it absorbed the electrons leaving only the unconverted gamma rays to produce the coincidence signal. Using this procedure, the response of the organic detector to the two electron lines was found to be approximately Gaussian in shape.

The electron source was constructed by placing the Bi^{207} between two pieces of Mylar tape which were then thermally fused together. The resulting source was optically transparent and degraded the electrons by only 0.005 MeV.

In determining the full width at half-maximum (FWHM), it was necessary to use twice the lower half width rather than the actual FWHM because of the distortion produced by the L conversion electrons of 0.554 and 1.049 MeV.

The characteristics of these electron spectra as observed by the liquid scintillator are given in Table III for several source positions. The peak position and FWHM measured for several radial positions were weighted by their corresponding detector volumes and a composite absorption spectrum was constructed for each source. These composite spectra are approximately Gaussian in shape and have resolutions of 43% and 31%, respectively, for the 0.472-MeV and 0.967-MeV electrons. There is a correction to the resolution measurements because they were made with a liquid scintillation detector amplifier gain of $\times 16$ while the main experiment was performed with an amplifier gain of $\times 8$. It was found that the FWHM spread of a pulser spectrum which was less than one channel at $\times 8$ was increased to 3 channels at $\times 16$ within the range of 0.50 to 4.0 MeV. This correction on the FWHM gives 33% and 25% for the scintillator resolution at 0.472 MeV and 0.967 MeV, respectively. These resolutions are consistent with those expected from photon statistics[14] and hence can be written as proportional to $E^{-1/2}$. Accordingly, the full width, W, which is the FWHM in MeV for an electron of kinetic energy E, can be written as $W=K\sqrt{E}$ where K is determined by the above data to be $=0.25$.

TABLE III. Response of target to electrons.

Electron energy =0.472 MeV			Electron energy =0.967 MeV		
Radial position (cm)	Peak channel	FWHM (channels)	Radial position (cm)	Peak channel	FWHM (channels)
0	28.0±1	13	0	55.5±1	19
5.1	30.5±1	14	5.1	57.0±1	19
8.9	29.0±1	13	8.9	58.5±1	19
12.0	34.0±1	13	12.0	67.0±1	19

Other calibration points were measured using the Compton recoil peak produced by the gamma rays from Cs^{137}, and the end point (3.54 MeV) of the beta spectrum from K^{42} decay. The Compton recoil peak from Cs^{137} has an energy of 0.43 MeV and a pulser setting of $(0.47\pm0.01)\times\frac{1}{5}$ matched the peak location. The Bi^{207} K conversion peaks as measured above correspond to pulser settings of $(0.55\pm0.01)\times\frac{1}{5}$ and $(1.15\pm0.02)\times\frac{1}{5}$ for the 0.472-MeV and 0.967-MeV lines, respectively.

The K^{42} source was made identical to the Bi^{207} source except for the use of 2.0 mg of separated K^{41}.[15] The Mylar-clad K^{41} sample was irradiated[16] in the thermal beam of a Savannah River Plant test reactor to produce an activity of ~ 0.1 μCi. Since the detector response was found to be nearly independent of the source position for an immersed source, a standard radial position of 7.5 cm was chosen for spectral measurements. The electron spectrum end point was obtained by using a Kurie plot of the form[17]

$$\left[\frac{N(W)}{\alpha F(-Z,W)W(W^2-1)^{1/2}}\right]^{1/2}=W-W_0,$$

where $W, N,$ and $F(-Z,W)$ are, respectively, the electron energy in mc^2 units, the number of electrons observed in the interval dW at W and the Coulomb factor. The shape factor α is of the form

$$\alpha=L_0(W_0-W)^2+9L_1,$$

where L_0 and L_1 have been tabulated.[18] After taking

[13] R. A. Ricci, Physica **23**, 693 (1957).

[14] A 0.98-MeV electron absorbed by the liquid scintillator produces approximately 6.5×10^3 photons. Assuming no absorption by the liquid scintillator and no reflections from the walls, 9.4% of the photons will fall on the photocathode producing, with a 10% photocathode efficiency, 60 photoelectrons. The FWHM resolution expected from photon statistics would therefore be $\approx 26\%$ $(\approx 2/\sqrt{60})$.

[15] 2 mg of separated K^{41} were obtained from Oak Ridge National Laboratory.

[16] We thank Dan Pellarin for source irradiation at the Savannah River Plant, Aiken, South Carolina.

[17] L. Pohm, Phys. Rev. **101**, 1315 (1956).

[18] M. E. Rose, Oak Ridge National Laboratory, Report No. 1459, 1953 (unpublished).

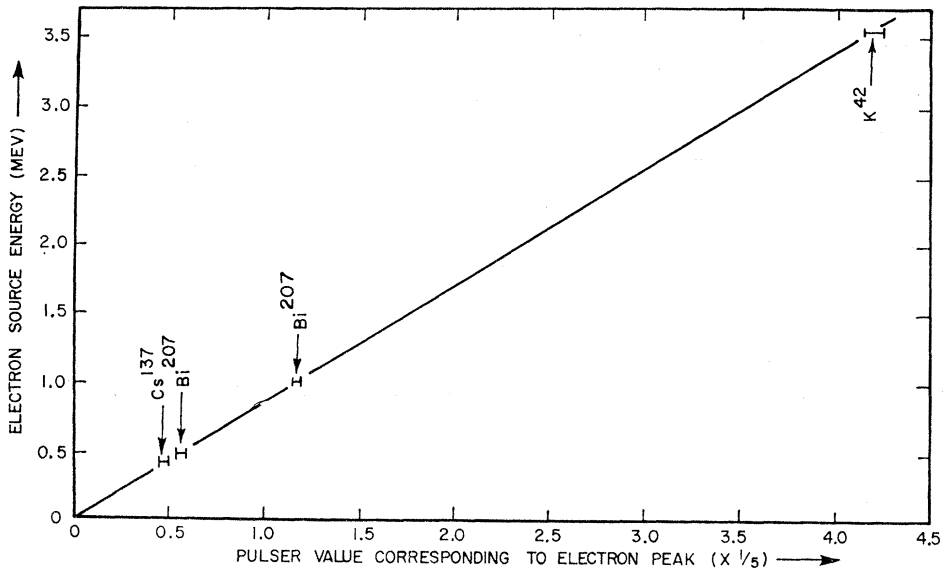

FIG. 8. Energy calibration of the liquid scintillation detector.

into account the energy resolution of the system, the Kurie plot gave an end point of $(4.18\pm0.05)\times\frac{1}{5}$ pulser units.

The linearity of the system is represented in Fig. 8. The precision with which the 3.54-MeV calibration fits the energy calibration curve verifies the experimentally obtained full-width resolution function from 0.5 to 3.5 MeV.

OPERATIONAL CALIBRATION OF THE DETECTOR

2841 h of data were collected for this experiment during a period of seven months. It was found to be necessary to "tune" the system and calibrate the detectors every 60 h. The tuning consisted of adjusting the position and width of the NaI window discriminators and the position of the integral discriminator level for the liquid scintillation system.

Because of temperature-dependent drifts in the NaI window discriminator circuits, the windows were set from $\frac{1}{10}$ to $\frac{1}{10}$ of the amplitude of the Gaussian photopeak produced by a 0.51-MeV gamma ray absorbed by the crystals. With the windows set this wide, 97.5% of the annihilation gamma rays absorbed by one crystal fell within the window and the drifts in 60 h produced a variation of less than $\pm1.2\%$. The detectors were calibrated by placing a Cs^{137} source on the crystal axis between NaI 1 and the organic detector (Fig. 1). A precision pulser was used to set the NaI window discriminators. The source produced in the liquid scintillator a spectrum whose peak fell at 0.43 MeV as calculated from the energy of the internal conversion line of a Cs^{137} source immersed in the liquid scintillator. This 0.43-MeV peak was used as the secondary standard to calibrate the liquid scintillator because (1) it did not have to be immersed in the liquid scintillator and hence reduced the possibility of contamination and (2) the organic detector and the NaI detectors could all be calibrated with the source in only one position.

The data were collected by photographing oscilloscope traces (Fig. 2) when the signals from the three detectors triggered the discriminators and formed a prompt triple coincidence. Because of the wide NaI discriminator windows, the rate at which photographs were taken was ~28 per hour so that a 100-ft roll of film was used every 60 h. At the beginning and end of each roll the system was calibrated and tuned and energy calibration pulses were recorded as was a time calibration consisting of pulses from a 100 kc crystal oscillator.

As a check on the NaI window and the target detector integral discriminator positions, the individual gate rates resulting from the natural background were measured and compared with previously measured rates. The coincidence rates between the two NaI crystals and each NaI crystal and the target detector were also measured.

The stability of the liquid scintillation detector system was determined during antineutrino runs by measuring the peak in the spectrum produced by cosmic-ray muons which passed through the detector. A separate monitoring amplifier (Fig. 5) was used to drive the pulse-height analyzer because the normal amplifier had a dynamic range up to 10 MeV while the through peak occurred at ~13 MeV. The cosmic-ray spectrum was accumulated continuously for seven days with a destructive printing of the spectrum from the pulse height analyzer every 12 h. Such a stability test was made once a month and the over-all gain of the liquid scintillation detector system was found to be stable to $\pm1\%$ over each seven-day period.

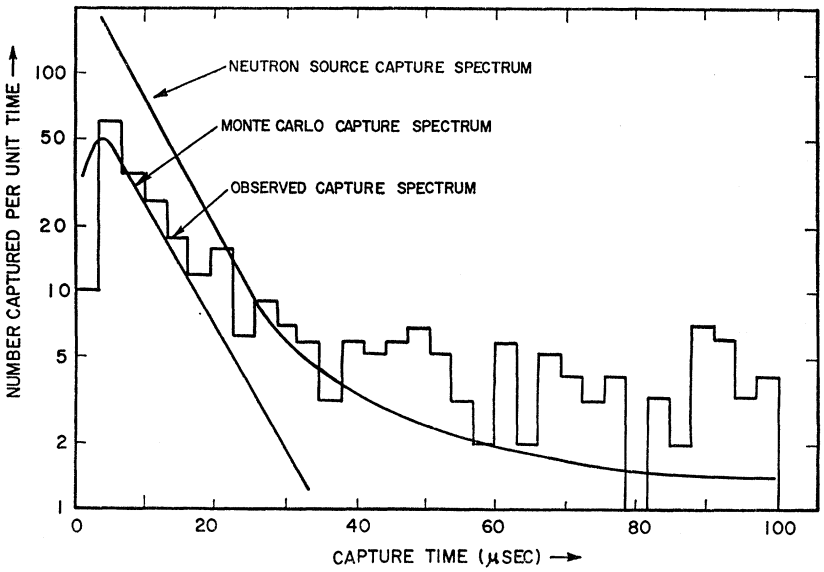

FIG. 9. Capture time spectra for neutrons in the liquid scintillation detector.

DEMONSTRATION THAT SIGNAL WAS CAUSED BY REACTOR ANTINEUTRINOS

The data consisted of oscilloscope traces as shown in Fig. 2. The class of events containing the signal consisted of a prompt triple coincidence plus a pulse with a time delay from 2.8 to 100 μsec. Because of the gadolinium concentration in the liquid scintillator, the delayed pulses produced by the neutrons capturing were predominantly (99%) contained in the first 50 μsec. The accidental delayed signals predominated in the second 50 μsec. The correlated signal is the rate in the first 50 μsec minus that in the second 50 μsec. The rate of the reactor-associated signal (RA signal), 0.187 $\pm$0.021/h, is then the difference between the reactor-up and reactor-down correlated rates.

Reactor-associated Signal is Not Produced by the Background from Reactor

First, we assume that a reactor associated neutron (either from fission or a photoneutron) produces the liquid scintillation detector signal and the gamma ray background triggers the two NaI detectors, and calculate the expected prompt triple coincidence rate. The measured coincidence rate between the NaI crystals is 1/min. If, as a gross overestimate, we attribute 50% of the reactor-associated liquid-scintillation-detector rate to neutron scatterings the neutron-induced liquid-scintillation-detector rate is <55/min. Using a coincidence resolution time of 2.0 μsec the prompt triple coincidence rate is calculated to be $<2.2\times10^{-4}$/h. Since the neutron capture probability was much less than 100%, this background would account for $<\frac{1}{10}$% of the observed reactor-associated signal.

Reactor neutrons unaccompanied by gamma rays can be ruled out as a source of background by the following straightforward argument.

If we allow for the inefficiency of a neutron to produce a pulse equal to that of a 0.5-MeV gamma ray in a NaI crystal it follows that a neutron of energy $\gtrsim$17 MeV was required to trigger one of the side crystals.[19] This means that a neutron with an energy >35 MeV was required to produce a prompt triple coincidence trigger and the ensuing delayed pulse. Such energetic neutrons are not associated with the reactor.

It is to be remarked that gamma rays unaccompanied by neutrons can produce only a readily recognizable uniform or noncorrelated distribution of time intervals for the delayed coincidence pulses.

Reactor-Associated Signal Shows Expected Characteristics

If the reactor-associated signal was produced by reaction (1), then the target-detector pulse-height distribution in the prompt triple coincidence should be consistent with the expected positron spectrum and the capture-time spectrum for the second pulse should be that of the liquid scintillation detector for neutrons.

To obtain a neutron capture-time spectrum for the gadolinium loaded liquid scintillation detector, a Pu-Be neutron source was placed within the organic detector on the axis and midway between the crystals. The capture times were measured by triggering a 100-μsec oscilloscope sweep each time one of the NaI crystals absorbed a 4.43-MeV gamma ray which accompanied the birth of 60% of the source neutrons. The result of the analysis of 10 200 traces obtained using the

[19] The maximum recoil energy E of Na struck by a neutron of energy E_0 is given by the well-known relation

$$E/E_0=1-[(A-1)/(A+1)]^2,$$

where for Na, $A=23$. The response of NaI to Na nuclei may be inferred from the papers of S. Bashkin *et al.*, Phys. Rev. **109**, 434 (1958).

Pu-Be source is the capture-time spectrum shown in Fig. 9.

Also presented on Fig. 9 is the capture-time spectrum obtained from 2484 h of antineutrino runs. When corrected for background this spectrum has a slope which is proportional to the mean capture time in the scintillator and is consistent with the slope of the spectrum obtained with the neutron source. Figure 9 also displays the capture-time spectrum calculated by a Monte Carlo method for 20 keV neutrons produced uniformly in the target. The mean capture times from all three spectra are consistent. It is therefore concluded that the second pulse of the reactor associated signal was produced by a neutron.

To associate the first pulse of the signal with the positrons expected from reaction (1), the following support is given. First, it has been shown that the background could not produce the observed correlated signal. Second, the energy spectrum of the first pulses in the organic detector is not consistent with the background seen by this detector (Fig. 10). Third, the organic detector spectrum is consistent with the shape expected from the known dependence on energy for the interaction cross section and a monotonically decreasing fission antineutrino spectrum.

DETECTION EFFICIENCY AS A FUNCTION OF ENERGY

Consider the target to be divided into thin cylindrical slabs, each at a distance x_i from the target center. The detection efficiency, $\eta(E)$, for the entire target can then be written[20] as

$$\eta(E)=\sum_i \eta_{\beta^+}(x_i,E)\eta_n(x_i)\,,$$

where

$\eta_{\beta^+}(x_i,E)$ = probability of detecting a positron of energy E produced in slab x_i,

$\eta_n(x_i)$ = probability of detecting a neutron produced in slab x_i.

Positron Detection Efficiency

The positron detection efficiency is the probability that the composite detector will record a prompt triple coincidence when a positron, produced in the target, annihilates. Since the triple coincidence is arranged to require energy deposits of at least 0.50 MeV in the organic detector and 0.51 MeV in each of the NaI crystals, this efficiency can be written in more detail as

$$\eta_{\beta^+}(x_i,E)=P_1(x_i,E)P_2P_3(x_i)+P_4(x_i,E)P_5(x_i,E)P_3(0)\,,$$

where

$P_1(x_i,E)$ is the probability that the positron will slow down and annihilate within the organic detector,

P_2 is the probability that the kinetic energy of the positron which annihilates in the organic detector is >0.50 MeV,

$P_3(x_i)$ is the probability that both annihilation gamma rays will escape from the organic detector without interacting and be totally absorbed by the NaI crystals,

$P_4(x_i,E)$ is the probability that the positrons which escape from the organic detector annihilate in the inert material between the target and the NaI crystals,

$P_5(x_i,E)$ is the probability that the electrons deposit >0.50 MeV in the organic detector before escaping.

The first term in the efficiency equation is due to positron annihilation within the target detector. The second term takes into account those positrons which escape from the target and annihilate in the inert material between the detectors to produce an acceptable triple coincidence. A detailed evaluation of these probabilities is given in Appendix II. The average positron detection efficiency was found to be 7.8%.

Neutron Detection Efficiency

The neutron detection efficiency, $\eta_n(x_i)$ is the probability that a neutron created in slab x_i will thermalize and capture within the detector system. The requirements imposed on the neutron capture signal are that the capture time t_c must be between $2.8\leq t_c<50$ μsec after the prompt triple coincidence signal and that the sum of the energy deposited in the three detectors for the neutron-capture signal must exceed 0.75 MeV. The average neutron detection efficiency was found to be 38%.

This efficiency could in principle be determined by using a low energy ($\sim$20 keV) neutron source which has a coincident gamma ray. However, low-energy neutron sources are in general accompanied by an excessive number of gamma rays.

Since we could not measure $\eta_n(x_i)$ directly, it was inferred from a combination of calculation and measurement using a Pu-Be source. The efficiency is given as the product of several terms.

$$\eta_n(x_i)=P_6(x_i)P_7P_8\,,$$

where

$P_6(x_i)$ is the probability that the neutrons produced in slab x_i will be captured within the detection system,

P_7 is the probability that the neutron will capture within the time gate of 2.8 μsec $\leq t_c<50$ μsec,

P_8 is the probability that the capture gamma rays will deposit a total energy in the three detectors in excess of 0.75 MeV.

These factors are discussed in Appendix III.

[20] Dr. Chudakov of the Lebedev Institute made a helpful comment regarding the interdependence of the positron and neutron detection efficiencies.

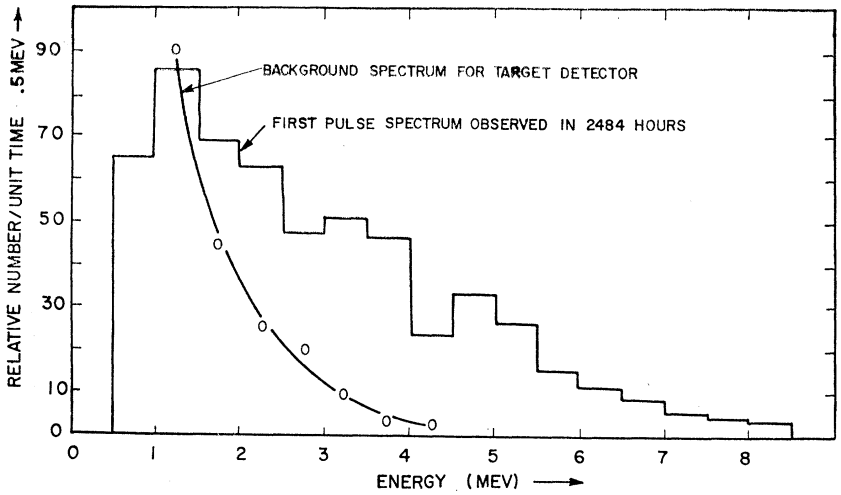

FIG. 10. Comparison of the positron and background energy spectra.

Energy Dependence of the Over-all Detection Efficiency, η

Collecting the numerical results from the previous sections:

$$\eta(x_i,E)=(0.78\pm0.06)P_1(x_i,E)P_3(x_i)P_6(x_i) + (0.061\pm0.004)P_4(x_i,E)P_5(x_i,E)P_6(x_i)\,.$$

To determine the energy dependence of η it was necessary to evaluate $\eta(x_i,E)$ for each x_i slab from 0.175 cm to 3.325 cm in steps of 0.35 cm for each positron energy from 0.75 MeV to 8.25 MeV. A sample of the results for $E=2.75$ MeV is presented in Table IV. $\eta(x_i,E)$ was summed over the x_i slabs for fixed E and the resultant energy dependence of the efficiency, $\eta(E)$, is shown in Table V.

TABLE IV. Numerical results of detection efficiency terms for $E=2.75$ MeV.

x_i (cm)	P_1 (%)	$P_3/(0.076\pm0.001)$	P_4 (%)	P_5 (%)	P_6 (%)	$\eta(2.75)$ (%)	$\Delta\eta$ (%)
0.175	97.1	1.33	0.00	100	58.7	4.50	0.351
0.525	97.1	1.29	0.00	100	58.0	4.31	0.336
0.875	97.1	1.25	0.00	100	55.5	4.01	0.316
1.22	97.1	1.22	0.00	100	55.0	3.85	0.306
1.57	97.1	1.18	0.00	100	54.0	3.67	0.291
1.92	97.1	1.14	0.00	100	48.1	3.17	0.254
2.27	85.2	1.11	9.97	100	43.6	2.71	0.200
2.62	74.3	1.08	21.4	100	38.6	2.34	0.157
2.97	63.5	1.04	32.6	100	33.0	1.96	0.123
3.32	52.7	1.01	32.6	81.2	22.8	1.09	0.072

THEORETICAL CROSS SECTION FOR MONOENERGETIC ANTINEUTRINOS

The cross section, $\sigma(E)(\text{cm}^2)$, for the absorption of monoenergetic antineutrinos of energy, E(MeV), by a free proton can be written[8] as

$$\sigma(E)=(2.23\pm0.05)\times10^{-44}\left\{\frac{E-1.29}{0.26}\right\}\times[(E-1.29)^2-0.26]^{1/2}. \quad (2)$$

The cross section was derived using the two component neutrino theory and inserting the measured neutron half-life[21] of 16.9±0.4 min and the Fermi function $F(\eta_0)=1.689$.[22]

POSITRON AND ANTINEUTRINO SPECTRA

We are now in a position to analyze the data and deduce the antineutrino spectrum from fission and the cross section for reaction (1) averaged over the fission spectrum.

In the 2484 h of reactor-up data, 928 events satisfied the selection criterion for reaction (1). These events were separated into two classes depending on whether their delayed pulses occurred in the first or second 50 μsec interval. The liquid scintillation detector first-pulse spectra associated with these time intervals are given in Table VI for 0.5 MeV intervals together with the correlated positron spectrum, i.e. the difference between these two spectra.

TABLE V. Energy dependence of detection efficiency, $\eta(E)$.

Position energy (MeV)	Detection efficiency (%)
0.75	3.27±0.27
1.25	3.25±0.27
1.75	3.23±0.27
2.25	3.20±0.26
2.75	3.17±0.26
3.25	3.11±0.25
3.75	3.05±0.25
4.25	2.97±0.24
4.75	2.89±0.23
5.25	2.80±0.22
5.75	2.70±0.21
6.25	2.62±0.20
6.75	2.54±0.19
7.25	2.46±0.19
7.75	2.38±0.18
8.25	2.30±0.17

[21] A. N. Sosnovsky, P. E. Spivak, Yu. A. Prokofiev, I. E. Kutikov, and Yu. P. Dobrinin, Nucl. Phys. **10**, 395 (1959).

[22] L. Durand, III, L. F. Landovitz, and R. B. Marr, Phys. Rev. Letters **4**, 620 (1960).

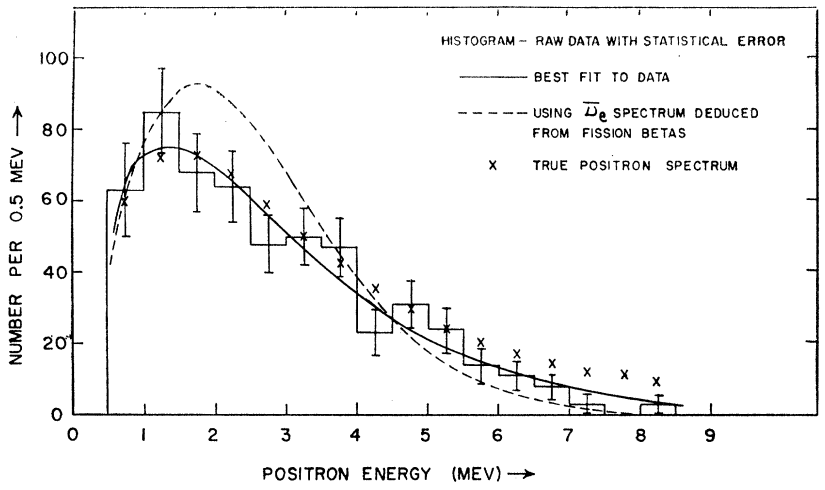

FIG. 11. Positron spectra from the reaction $p(\bar{\nu}_e, \beta^+)n$. The abscissa is the kinetic energy of the β^+. To obtain the energy of the associated $\bar{\nu}_e$ add 1.80 MeV.

The corresponding reactor-down (357 h) spectra are also given in Table VI. The correlated reactor-down spectrum represents 15% of the correlated reactor-up signal rate and is, in consequence, very poorly determined. We therefore neglect this correction to the positron spectrum except to note that the meager reactor-down data are grouped at the lower energies and hence the ensuing analysis probably gives a maximum in the β^+ spectrum at an energy which is slightly too low.

We assumed a two-parameter expression for the "true" positron spectrum (Appendix IV), and determined the best values for these parameters by minimizing the sum of the squared residuals between the observed positron spectrum and the "true" positron spectrum modified by the resolution and detection efficiency. The "true spectrum" is the product of the cross section the energy dependence of which is believed to be given by the phase space available to the positron, and an expression for the $\bar{\nu}_e$ flux which contains two parameters and the general features indicated by earlier measurements of the electron spectrum from fission fragments.[23,24] Figure 11 shows the measured positron spectrum without corrections, the fitted spectrum, and the fitted spectrum modified for detector resolution and efficiency. Also shown is the spectrum which we predicted by using the antineutrino spectrum determined by inverting the fission electron spectrum[23] and the cross section of Eq. (2). An important feature of the positron spectrum we measured is the noticeable departure above 4 MeV from the spectrum predicted from measurements of fission electrons. This comparison indicates a larger number of fission antineutrinos above 6 MeV than previously expected.[25]

TABLE VI. First-pulse energy spectra.

Energy (MeV)	Reactor-up spectra (2484 h) (a) Capture in first 50 μsec	(b) Capture in second 50 μsec	Reactor-up Correlated (a−b)	Reactor-down spectra (357 h) Capture in first 50 μsec	Capture in second 50 μsec
0.75	115	52	63	8	6
1.25	116	31	85	4	1
1.75	94	26	68	1	3
2.25	87	23	64	1	1
2.75	59	11	48	2	0
3.25	63	13	50	2	0
3.75	56	9	47	1	0
4.25	33	10	23	2	0
4.75	35	4	31	0	1
5.25	31	7	24	0	0
5.75	20	6	14	0	0
6.25	15	4	11	0	0
6.75	11	3	8	1	1
7.25	5	2	3	0	0
7.75	2	2	0	1	0
8.25	5	2	3	1	0
>8.50	18	11	7	2	1

The unnormalized fission antineutrino spectrum obtained from the best fit of the data is

$$n(E) = Ae^{-(1.28\pm0.02)E+(0.0402\pm0.0002)E^2}, \qquad (3)$$

where E is in MeV. The uncertainty in the exponent arises from the uncertainty in the determination of the detection efficiency as a function of energy. The normalization, A, of the antineutrino spectrum is determined from the fission electron spectrum measurement of Wyman and Kutcher[25] which gave 2.1±0.1 antineutrinos per fission with energies in excess of 1.80 MeV. The normalization is calculated to be $A = 19.4\pm1.3$ where the uncertainty in both normalization of the fission beta spectrum and the determined antineutrino spectral shape, Eq. (3), are included. It must be noted that this expression is presented as the best spectrum

[23] The best previously determined expression for the incident $\bar{\nu}_e$ energy (Ref. 24) spectrum was obtained by least-square fitting the data of Carter, *et al.*, for the $\bar{\nu}_e$ spectrum calculated from the beta spectrum from U^{235} fission. The expression obtained for the number of $\bar{\nu}_e$ per fission per MeV which is valid for 1.0 MeV$\leq E<$8.5 MeV is $f(E)=5.01\exp(-0.505E-0.0544E^2)$.

[24] R. E. Carter, F. Reines, R. Wagner, and M. E. Wyman, Phys. Rev. **113**, 208 (1959).

[25] This conclusion is supported by recent measurements of the fission electron spectrum made by M. E. Wyman and J. Kutcher. We are indebted to Professor Wyman for communication of these results prior to publication.

we can deduce from our data and that it has validity only in the range $1.8 \leq E < 10.0$ MeV. The divergence at large E of this semiempirical expression for $n(E)$ has no physical significance. The direct determination of the antineutrino spectrum made here avoids the question, except for normalization, of the uncertainties in the process of deducing the $\bar{\nu}_e$ spectrum from the fission beta spectrum. This inversion is uncertain to the extent that the charge distribution of fission fragment β emitters is uncertain. In addition, because of the quadratic rise of the cross section for our reaction with $\bar{\nu}_e$ energy, a direct measurement of the spectral shape accentuates the spectrum at higher energies as compared with a measurement of the fission betas.

REACTION CROSS SECTION

The average cross section per fission antineutrino for the reaction $P(\bar{\nu}_e,\beta^+)n$ that one would predict using Eq. (2) for the energy-dependent cross section and Eq. (3) for the fission-antineutrino spectrum is

$$\bar{\sigma}_{\text{th}} = (1.07 \pm 0.07) \times 10^{-43} \text{ cm}^2/\text{fission } \bar{\nu}_e ,$$

where the uncertainty[26] results primarily from the normalization of Eq. 3.[27]

The cross section deduced from this experiment can be expressed as

$$\bar{\sigma} = (R/3600 f N \bar{\eta}) ,$$

where R = observed reactor-associated signal rate (h^{-1}), f = antineutrino flux incident on the detector 7.2×10^{13} ($\text{cm}^{-2}\,\text{sec}^{-1}$), N = total number of target protons $= 2.56 \times 10^{26}$, $\bar{\eta}$ = detection efficiency averaged over the spectrum $= 0.030 \pm 0.002$. The reactor-up and reactor-down associated signal rates are, respectively, $(549 \pm 31)/2484$ h and $(12 \pm 6.3)/357$ h, giving $R = (0.187 \pm 0.021)$/h. The average cross section is therefore

$$\bar{\sigma}_{\text{exp}} = (0.94 \pm 0.13) \times 10^{-43} \text{ cm}^2 .$$

SIGNIFICANCE OF RESULTS

The ratio of the average cross section per fission antineutrino determined from this experiment to that expected from the two-component neutrino theory is

$$\bar{\sigma}_{\text{exp}}/\bar{\sigma}_{\text{th}} = 0.88 \pm 0.13 .$$

This ratio[28] is consistent with unity and not with the value two required by the four-component theory. Hence this experiment supports the validity of the two-component neutrino theory and rules against the predictions made before the downfall of the concept of parity conservation in weak interactions.[2]

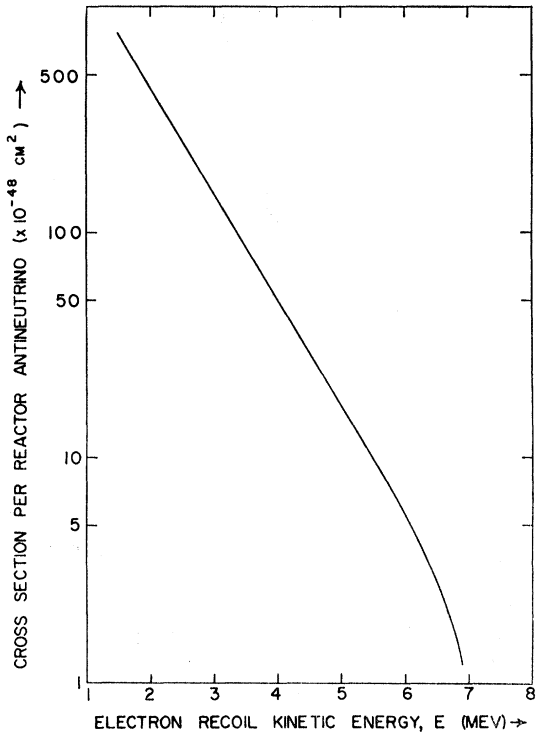

FIG. 12. Cross section for reactor antineutrinos to produce recoil electrons in excess of energy E via reaction (5).

Using the fission antineutrino spectrum (Eq. 3) it is possible to obtain the average cross section per fission antineutrino for two reactions which are being investigated[29] using fission antineutrinos. These reactions are

$$\bar{\nu}_e + d \rightarrow \beta^+ + n + n , \tag{4}$$

$$\bar{\nu}_e + \beta^- \rightarrow \bar{\nu}_e + \beta^- . \tag{5}$$

The difficulties and importance of observing these reactions have been pointed out previously.[30]

Reaction (4) with a threshold of 4.0 MeV is very sensitive to the shape of the higher energy portion of the antineutrino spectrum. Using the cross sections calculated by Weneser,[31] the fact that $\sigma(E/(E-4.0)^2$ is a relatively smooth function, a tensor coupling constant of $3g_t^2 \simeq 4.0 \times 10^{-23}$ and a factor-of-2 enhancement to take the two-component theory into account we calculate the average cross section per fission antineutrino to be

$$\bar{\sigma} = (4.2 \pm 1.4) \times 10^{-45} \text{ cm}^2 .$$

In considering an experimental observation of the antineutrino electron scattering reaction (5) it appears

[26] We quote where possible rms errors. Elsewhere we list the *extremes* of our uncertainties. Therefore the quoted uncertainties in the results are larger than rms.

[27] The average cross section $\bar{\sigma}_{1.80}$ per fission antineutrino above 1.80 MeV is better determined, since it is independent of the antineutrino spectrum normalization: $\bar{\sigma}_{1.80} = (3.12 \pm 0.32) \times 10^{-43}$ cm^2.

[28] The first determination of this ratio by F. Reines and C. L. Cowan, Phys. Rev. **113**, 223 (1959), gave $\bar{\sigma}_{\text{exp}}/\bar{\sigma}_{\text{th}} = 1.1 \pm 0.3$.

[29] Preliminary results have been obtained from the deuteron reaction by T. L. Jenkins and one of us (F. R.) (unpublished).

[30] F. Reines, Ann. Rev. Nucl. Sci. **10**, (1960), and C. L. Cowan and F. Reines, Phys. Rev. **107**, 1609 (1957).

[31] J. Weneser, Phys. Rev. **105**, 1335 (1957).

that it will be necessary to observe electrons with recoils above 1.5 MeV in order to discriminate sufficiently against background. The cross section per fission antineutrino for producing electron recoils in excess of a given energy was calculated by using the total cross section given by Feynman and Gell-Mann[32] with the correct two component neutrino coupling constant, $\sigma_0=16.6\times10^{-45}$ cm^2, and the electron recoil spectrum, $n(E_{\bar{\nu}_e}, E_{\beta^-})$, as a function of antineutrino energy

$$n=\left(\frac{E_{\bar{\nu}_e}}{0.51}-\frac{E_{\beta^-}}{0.51}\right)^2\Big/\left(\frac{E_{\beta^-}}{0.51}+1\right)^2,$$

where the energies are in MeV. Figure 12 shows the cross section for production by a fission $\bar{\nu}_e$ of recoil electrons with an energy $>E$ MeV.

It is possible to make two comments on the fission process using the antineutrino spectrum measured in this paper. First, the presence of antineutrinos up to $\sim$9 MeV corresponds to half-lives of 60 msec for allowed or to 10 msec for superallowed decays. These half-lives are shorter than previously reported.[33]

Second, the measured beta spectrum from fission fragments differs from the corresponding antineutrino spectrum because of the finite mass of the electron and the Coulomb distortion produced between the electron and the nucleus. By comparing the beta spectrum with the antineutrino spectrum it should be possible to comment on the average charge of short-lived fission fragments undergoing beta decay.

In view of the foregoing it would be useful to make an even more precise measurement of the positron spectrum than that described in the present paper.

SYSTEM IMPROVEMENTS

Background Analysis

The primary improvement that can be made in this experiment is to reduce the prompt triple coincidence background. This background, which is $\sim$28/h, cannot be produced by accidental triple coincidences or the combination of a double Compton scattering of a gamma ray in two detectors and an accidental in the third detector. Also, pair production in the organic detector can produce at most two triple coincidences per hour. One of the mechanisms which *can* produce this background is recoil electrons which are driven between adjacent detectors.

The prompt triple coincidence background in this case is estimated to be produced by a gamma ray which Compton scatters in two detectors, driving one of the electrons into the third detector. The electrons in passing through the inert matter between the detectors will lose 1.90 MeV, hence the driven electron must possess a minimum initial energy of 2.90 MeV. The gamma threshold for producing the driven electron and the coincident second scattering is $\sim$4.2 MeV, a number which is obtained by using the relationship connecting the gamma energy and the average kinetic energy of the Compton electron.[34]

The gamma flux incident on the organic detector was obtained from the NaI background spectrum after the spectrum was corrected for the response of the crystal.[35] Knowing the incident gamma-ray spectrum, the Compton cross sections and the total number of target electrons, the rate at which recoil electrons were driven through the detector and satisfied the energy requirements was estimated to be $\sim$10/h. This source of background could be eliminated by inserting thin plastic scintillation sheets between the detectors as an anticoincidence for the driven electron-produced events. Another possible source of background triples is the capture of neutrons in the vicinity of the detector.

Virtues of Reducing the Prompt Triple Coincidence Background

If the triple coincidence background can be sufficiently reduced, many advantages can be realized. With a higher signal-to-background ratio for the prompt pulse, a larger fraction of the photographs taken would contain delayed events resulting in reduced data handling and film consumption.

Although we have not done so in the present experiment, use could be made of the fact that the energies of the NaI crystal pulses for a prompt coincidence determine a point in the E_1, E_2 space where E_1 and E_2 are the energies of the NaI 1 and NaI 2 pulses, respectively: the positron events in the vicinity of 0.5 produce a peak in this space and thus 0.5 MeV can be used to discriminate against the coincidences not produced by positrons. If the background can be reduced sufficiently, it may be possible to identify inverse beta decay events by the positron signal alone so that:

(a) A higher signal rate would result, since it is not reduced by the neutron detection efficiency.

(b) The detection efficiency would be just the positron efficiency and hence could be more easily determined with precision.

(c) Inverse beta decay reactions in which no neutron is produced could be investigated, e.g., $He^3(\bar{\nu}_e, \beta^+)H^3$.

ACKNOWLEDGMENTS

We wish to thank A. A. Hruschka for the design and construction of the platform, detector box, and lead shield. B. Shoffner was helpful in the design of various

[32] R. P. Feynman and M. Gell-Mann, Phys. Rev. **109**, 193 (1958).

[33] J. E. Brolley, Jr., D. H. Cooper, W. S. Hall, M. S. Livingston, and L. K. Schlacks, Phys. Rev. **83**, 990 (1951) placed an upper limit on all such short-lived activities of 5% the intensity of the 1-sec period activities.

[34] R. D. Evans, Ref. 12, p. 688.

[35] W. F. Miller, J. Reynolds, and W. J. Snow, Rev. Sci. Instr. **28**, 717 (1957).

electronic components, and Mrs. R. Alexander advised on coding and running some of the calculations on the Case 1107 Univac computer. Finally we express our appreciation to the DuPont Company for their hospitality and cooperation at the Savannah River Plant where these measurements were made.

APPENDIX I: OPTIMUM THICKNESS OF THE LIQUID SCINTILLATION DETECTOR

The liquid-scintillator thickness effects the observed prompt triple coincidence rate (TCR) for reaction (1) in three ways:

1. For a fixed detector radius, the number of targets and therefore the signal rate is linearly dependent on the detector thickness, t.

2. The probability, P_c, of containing positrons of energy E in the liquid scintillation detector and hence observing the full positron kinetic energy is from the geometry

$$P_c=0.75+0.25\left[\frac{(R-r)^2}{R^2t}(t-2r)\right],$$

where R and t are the detector radius and thickness, respectively. r is the distance from the point of origin to the annihilation position of the positron.

3. The probability that the two annihilation gamma rays will penetrate the liquid scintillator without interacting can be calculated by using the following approximation. Assume the target to be a slab of liquid scintillator of thickness t and infinite lateral extent placed between two half planes of NaI. This approximation is good to about $\pm 10\%$ for the central point of the detector because of the argument presented to justify the ∞-slab approximation in the P_3 determination in Appendix II. The optimum thickness determined from this model will be a good approximation to the optimum thickness of the actual detector for noncentral positions because the probability of the annihilation gamma rays escaping from the target without interacting is only appreciable for small θ, where θ is the angle between the γ-ray trajectory and the normal to the detector interface.

We can write the probability, P_A, of both annihilation gamma rays escaping the liquid scintillation detector for all positions between the NaI crystals and averaged over all solid angles as

$$P_A=\int_0^1 e^{-l/\lambda}d(\cos\theta)$$

where $l=t/\cos\theta$ is the total path length of the two γ rays through the target and λ is the interaction mean free path for 0.51-MeV gamma rays in the liquid scintillator.

The TCR can now be written as the product tP_cP_A,

$$\mathrm{TCR}=Kt\left\{0.75+0.25\frac{(R-r)^2}{R^2t}(t-2r)\right\}\times\int_0^1 e^{-t/\lambda\cos\theta}d(\cos\theta)$$

where K is a constant. Evaluating TCR as a function of t for the case of $R=17.8$ cm, $r=0.6$ cm (1.75-MeV positron) and $\lambda=12$ cm gives the desired dependence of the triple coincidence rate on the detector thickness, shown on Fig. 13. It is seen to be relatively independent of target thickness in the vicinity of the maximum.

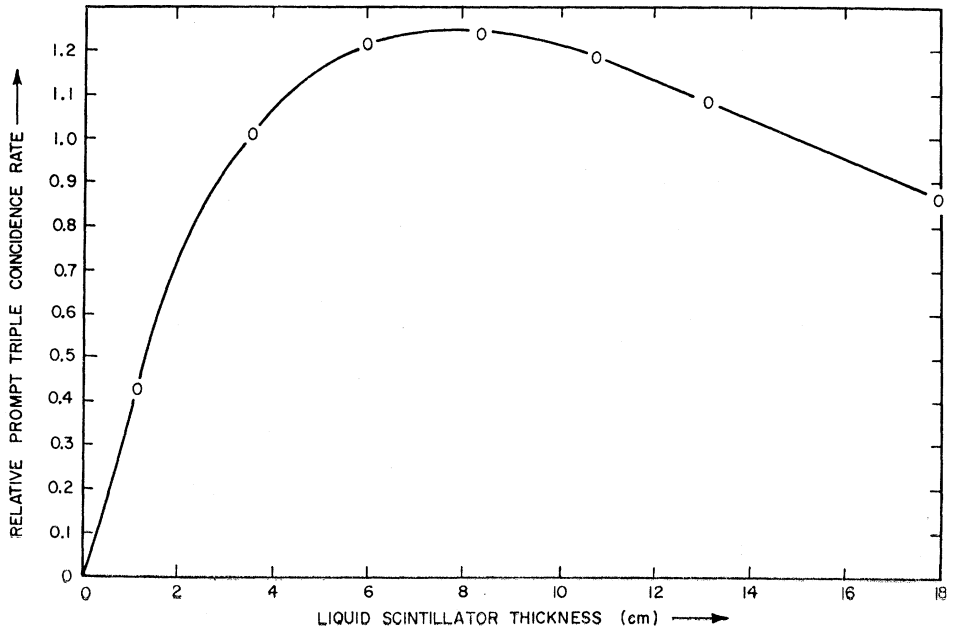

FIG. 13. Effect of liquid-scintillator thickness on prompt-triple-coincidence rate.

APPENDIX II: EVALUATION OF POSITRON EFFICIENCY TERMS P_1, $P_2 \cdots P_5$

$P_1(\chi_i,E)$

For a given positron energy E (MeV) the effective range, r (cm), is given[36] by

$$r=0.478E^{(1.265-0.094\ \ln E)} \quad \text{for} \quad E\leq 2.5\ \text{MeV}$$
$$=0.602(E-0.106) \quad \text{for} \quad E>2.5\ \text{MeV},$$

where we have included the liquid-scintillator density of 0.88 g/cm³. If a positron of range r is produced isotropically and at random in the slab χ_i, then the probability, P_1, that the positron will be contained within the target is approximately the fractional area of the sphere of radius r which lies inside the target. For the detector radius $Q=13.5$ cm and thickness 7.0 cm,

$$P_1(\chi_i,E)$$
$$=0.75+0.25(1-r/Q) \quad \text{for} \quad \chi_i\leq(3.5-r)$$
$$=\left\{1+\frac{3.5-\chi_i}{r}\right\}[0.375+0.125(1-r/Q)^2] \quad \text{for} \quad \chi_i>(3.5-r).$$

P_2

The probability that the kinetic energy of the positron which annihilates within the organic detector is in excess of 0.50 MeV is determined from the observed positron spectrum, Fig. 11. The spectrum is extrapolated to the origin and P_2 is the ratio of the area under the experimental spectrum to the area under the extrapolated spectrum, i.e.,

$$P_2=549/(574\pm10)=0.96\pm0.02.$$

The error reflects the uncertainty in the shape of the spectrum between 0.50 MeV and the origin. The error introduced into this factor by using the uncorrected positron spectrum is considered too small to warrant a more refined estimate.

P_3

The probability that both annihilation gamma rays will not interact in the organic detector but will be completely absorbed by the NaI crystals was inferred from measurements made with a Cu^{64} source and also calculated de novo. The source was calibrated by placing it centrally on the face of one NaI crystal and measuring the rate of events in the 0.51-MeV photopeak. Corrections were made to compensate for scattering in the inert front window of the crystal, back scattering from the crystal, and the crystal thickness.

The source was then placed within the target-detector liquid and the coincidence rate was measured between the two NaI crystals with the NaI window discriminators tightly set on the annihilation peaks. Its position was varied radially (r) and parallel (χ) to the detector axis of symmetry and the coincidence rate normalized to the source strength gives P_3, as listed in Table VII. Weighing the radial dependence of P_3 by the volume an average efficiency of $(7.6\pm0.1)\%$ is obtained for the $\chi=0$ slab. Finally

$$P_3(\chi_i)=(0.076\pm0.001)\times\left\{\left(\frac{1}{0.565}\right)\left[1-\frac{3.5+\chi_i}{[14.5^2+(3.5+\chi_i)^2]^{1/2}}\right]\right\} \quad \text{for} \quad 0\leq\chi_i\leq3.5.$$

TABLE VII. Dependence of P_3 on position within target.

Position (r,χ) (cm)	P_3 (%)
0.00, 0.00	13.0 ±0.1
0.00, 3.80	16.8 ±0.1
1.25, 0.00	12.8 ±0.1
5.00, 0.00	11.2 ±0.1
8.25, 0.00	10.8 ±0.1
10.00, 0.00	6.86±0.06
12.00, 0.00	1.97±0.02

Where the χ_i dependence reflects the variation of solid angle subtended by the more distant NaI detector normalized to the $\chi=0$ slab.

P_3, was also obtained from a calculation assuming the detectors to be their actual thicknesses but infinite in extent. For the position $\chi=0.0$ cm, the calculation gave $P_3=13.8\%$, which compares favorably with the experimentally obtained value of $13.0\pm0.1\%$.

The ∞-slab approximation yields only a slight overestimate for the value of P_3 because the gamma rays which traverse the liquid scintillator detector outside the solid angle subtended by the "actual NaI crystals" have such long path lengths in the scintillator that their probability of interacting before reaching the NaI crystals is very high. Therefore, these gamma rays which cannot contribute to P_3 in the actual detection system contribute very little to P_3 in the ∞-slab model because of their high probability of interacting in the liquid scintillator.

$P_4(\chi_i,E)$

The inert material between the organic detector and the NaI crystals includes the Lucite cover of the target, (0.085 cm) the stainless steel housing of the NaI crystals (0.048 cm) and the MgO packing around the NaI crystals (0.273 cm). The total thickness of inert material was 0.915 g/cm². This corresponds to an energy loss of 1.90 MeV or a distance traveled in the organic detector of 1.0 cm. $P_4(\chi_i,E)$ can now be written as

$$P_4(\chi_i,E)=P_4{}^aP_4{}^b,$$

where $P_4{}^a$ = probability that the positron escapes through the top or bottom of the target, $P_4{}^b$ = proba-

[36] L. Katz and A. S. Penfold, Rev. Mod. Phys. 24, 28 (1952).

bility that the positron which escapes from the target will not penetrate the inert material. $P_4{}^a$ includes only positrons which escape through the top and bottom of the target since those which escape through the side result in annihilations which cannot be detected by both crystals. Using the same method and notation as in the determination of $P_1(\chi_i,E)$, we obtain

$$P_4{}^a=0, \qquad \text{for} \quad \chi_i\leq 3.5-r$$
$$=0.50[1-(3.5-\chi_i)/r], \qquad \chi_i>3.5-r$$

and

$$P_4{}^b=1.0, \qquad E\leq 1.90 \text{ MeV}$$
$$=1.0, \qquad E>1.90\text{MeV}, \ \chi_i\leq 4.50-r$$
$$=1-\frac{1-(4.47-\chi_i)/r}{1-(3.5-\chi_i)/r}, \qquad E>1.90 \text{ MeV}, \ \chi_i>4.50-r.$$

$P_5(\chi_i,E)$

$P_5(\chi_i,E)$ is the probability that a positron which escapes from the target before annihilating deposits at least 0.50 MeV in the target. If r_1 and r are the ranges of electrons of energy 0.50 MeV and E MeV, respectively, then we can write

$$P_5(\chi_i,E)=1-\frac{1-(3.5-\chi_i)/r_1}{1-(3.5-\chi_i)/r} \quad \text{for} \quad \chi_i>(3.5-r_1)$$
$$=1.0 \quad \text{for} \quad \chi_i\leq(3.5-r_1).$$

APPENDIX III: EVALUATION OF NEUTRON EFFICIENCY TERMS P_6, P_7, P_8

$P_6(\chi_i)$

In order to determine the probability, $P_6(\chi_i)$, of the neutron capturing within the detection system as well as the variation of over-all detection efficiency with neutron energy, it was necessary to calculate the neutron slowing down diffusion and capture process for various locations in the liquid scintillation $\bar{\nu}_e$ target. The Monte Carlo technique[37] was employed in this calculation. Neutrons were followed from their birth position, which was chosen so as to correspond to a uniform volume distribution, in slab χ_i through successive scatterings until they either were captured in the detection system or escaped from it.

The cross sections were obtained from the Brookhaven neutron cross-section compilation,[38] except for the H_2 scattering cross sections which were taken from the work of Melkonian and Jones,[39] and the most current

[37] E. D. Cashwell and C. J. Everett, *Monte Carlo Method* (Pergamon Press, Inc., New York, 1959). Details of our calculation may be found in the Ph.D. thesis of F. A. Nezrick.

[38] Brookhaven National Laboratory Report 325 (U. S. Government Printing and Publishing Office, Washington 25, D. C.)

[39] E. Melkonian, Phys. Rev. **76**, 1750 (1949); W. B. Jones, Jr., Phys. Rev. **74**, 364 (1948).

TABLE VIII. $P_6(\chi_i)$ calculated by the Monte Carlo method.

χ_i (cm)	$P_6(\chi_i)$
0.175	0.587±0.027
0.525	0.580±0.027
0.875	0.555±0.026
1.225	0.550±0.026
1.575	0.540±0.026
1.925	0.481±0.024
2.275	0.436±0.022
2.625	0.386±0.021
2.975	0.330±0.019
3.325	0.226±0.015

I^{127} radiative neutron capture cross sections from Popov and Shapiro.[40]

The results of the Monte Carlo calculations are shown in Table VIII. Since 2 and 20 keV represent the energy limits of neutrons produced via Eq. (1) by fission antineutrinos, we introduced such neutrons into the system. The results were found to be the same at both limits and therefore $P_6(\chi_i)$ is independent of energy.

P_7

The probability of capturing the neutron in the time gate 2.8 μsec$\leq t_c\leq$50 μsec was obtained from the experimentally observed capture spectrum, Fig. 9. The shape of the capture time spectrum obtained from the Monte Carlo calculation was found to be independent of χ_i and was in good agreement with experiment. Assuming that the experimental spectrum goes smoothly to zero at the origin, as does the Monte Carlo spectrum, we obtain $P_7=0.92\pm0.01$.

P_8

When a neutron is captured by gadolinium, it produces, on the average, four gamma rays with mean energies of $\sim$2 MeV.[3] The probability of one of these gamma rays striking a NaI crystal is 0.61±0.03 averaged over the target volume. The probability of the gamma ray interacting in the detectors and depositing more than 0.75 MeV is 0.67±0.03. However, since four gamma rays, on the average, are emitted, and we require that they make a total energy deposit in excess of 0.75 MeV, $P_8=0.88\pm0.05$ for directionally uncorrelated gamma rays.

APPENDIX IV: RESOLUTION UNFOLDING AND LEAST-SQUARES FITTING OF THE POSITRON SPECTRUM

The calculation of the spectral distortion due to a resolution function of a detector is a problem which has been formulated elsewhere.[41,42] In the present case we

[40] Y. P. Popov and F. L. Shapiro, Zh. Eksperim. i Teor. Fiz. **42**, 988 (1962) [English transl.: Soviet Phys.—JETP **15**, 683 (1962).

[41] G. E. Owen and H. Primakoff, Rev. Sci. Instr. **21**, 447 (1950).

[42] M. S. Freedman, T. B. Novey, F. T. Porter, and F. Wagner, Jr., Rev. Sci. Instr. **27**, 716 (1956).

are concerned with the inverse problem, i.e. the distorted spectrum (the observed positron spectrum) and the resolution function of the liquid scintillation detector are known and it is desired to obtain the true positron spectrum. The distortion of a spectrum by a resolution function can be expressed as

$$M(E)=\int_0^{E_{\max}} N(E')L(E,E')dE',$$

where $M(E)dE$=number of events observed with energy between E and $E+dE$, $N(E')dE'$=number of events with true energy between E' and $E'+dE'$, $L(E,E')dE$=the probability of observing between E and $E+dE$ a particle whose true energy is E'.

The resolution function of the liquid scintillation detector was determined to be approximately a Gaussian with an energy-dependent half-width given by FWHM$=K\sqrt{E}$.

Therefore,

$$L(E,E')=\frac{1}{K(\pi E')^{1/2}}\exp\left(-\frac{(E'-E)^2}{K^2E}\right).$$

The true spectrum is assumed not to be grossly different in shape from the predicted spectrum which is the product of the cross section, Eq. (2), and the general form of the antineutrino spectrum determined from the fission beta spectrum. The true positron spectrum can be written in an un-normalized form as

$$N(E)=e^{bE+cE^2}(E-1.29)\{(E-1.29)^2-0.26\}^{1/2}, \quad (6)$$

where $b=-0.505+\delta b$, $c=-0.0544+\delta c$, E=neutrino energy in MeV.

The parameters δb and δc which are deviations from the previously determined antineutrino spectrum can vary the location of the peak and the shape of the spectrum.

Since the resolution unfolding is done by a machine calculation it is expedient to perform the least-squares fitting of the data and resolution unfolding together. The least-squares fitting is performed by minimizing the quantity, $\mathfrak{L}$,

$$\mathfrak{L}=\sum_i\left[M(E_i)-\int_0^{E_{\max}} N(E')L(E_i,E')dE'\right]^2.$$

It has been determined in previous calculations that there is little advantage in taking weighted residuals; therefore this was not done here. Taking into account the finite width (0.50 MeV) of the histogram intervals comprising the positron spectrum and the energy dependence of the detection efficiency, $\mathfrak{L}$ can be written as

$$\mathfrak{L}=\sum_i\left\{M(E_i)-\frac{\chi}{\chi'}\int_0^{10.8} e^{bE'+cE'^2}P(E_i)\times(E-1.29)[(E-1.29)^2-0.26]^{1/2}\times\int_{E_i-0.25}^{E_i+0.25}\frac{\exp[-(E'-E_i)^2/K^2(E'-1.8)]}{K[\pi(E'-1.8)]^{1/2}}dE_idE'\right\}^2.$$

where

$$\chi=\sum_i M(E_i),$$

$$\chi'=\sum_i\int_0^{10.8} e^{bE'+cE'^2}P(E_i)(E-1.29)\times[(E-1.29)^2-0.26]^{1/2}\times\int_{E_i-0.25}^{E_i+0.25}\frac{\exp[-(E'-E_i)^2/K^2(E'-1.8)]}{K[\pi(E'-1.8)]^{1/2}}\times dE_idE'$$

$P(E_i)$=total detection efficiency for energy E_i.

The term χ/χ' is necessary for renormalization of the true spectrum. Since the unfolded spectrum was assumed not to differ greatly from the predicted spectrum the minimum value of $\mathfrak{L}$ was found by searching the δb, δc space in the vicinity of $\delta b=\delta c\sim 0$. The minimum was actually found at $b=-1.28$ and $c=+0.0402$. The maximum effect on b and c of the uncertainty in the total detection efficiency, $P(E_i)$, was obtained by using for $P(E_i)$ two smoothly varying functions with the greatest difference in shape allowed by the uncertainty. One function chosen varied smoothly from $P(2.55)+\Delta P(2.55)$ to $P(10.05)-\Delta P(10.05)$ while the second function varied from $P(2.55)-\Delta P(2.55)$ to $P(10.05)+\Delta P(10.05)$ where the efficiencies, $P(E_i)$, and the uncertainties in the efficiencies, $\Delta P(E_i)$, are given in Table V. These functions gave variations in b, c which we take as the error in their determination:

$$b=-1.28\pm 0.02,$$
$$c=0.0402\pm 0.0002.$$